

# Visualizing Electromagnetic Fields at the Nanoscale by Single Molecule Localization

Christian Steuwe,<sup>†,‡</sup> Miklos Erdelyi,<sup>†</sup> G. Szekeres,<sup>§</sup> M. Csete,<sup>§</sup> Jeremy J. Baumberg,<sup>‡</sup> Sumeet Mahajan,<sup>\*,||</sup> and Clemens F. Kaminski<sup>\*,†</sup>

<sup>†</sup>Department of Chemical Engineering and Biotechnology, University of Cambridge, New Museums Site, Pembroke Street, Cambridge CB2 3RA, U.K.

<sup>‡</sup>Nanophotonics Centre, Cavendish Laboratory, University of Cambridge, JJ Thomson Avenue, Cambridge CB3 0HE, U.K.

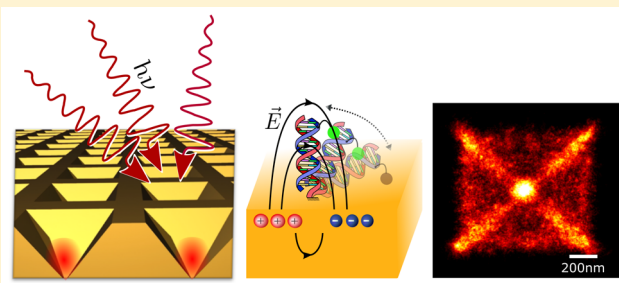
<sup>§</sup>Department of Optics and Quantum Electronics, University of Szeged, H-6720 Szeged, Dóm tér 9, Hungary

<sup>||</sup>Institute for Life Sciences and Department of Chemistry, University of Southampton, University Road, Southampton SO17 1BJ, U.K.

## Supporting Information

**ABSTRACT:** Coupling of light to the free electrons at metallic surfaces allows the confinement of electric fields to subwavelength dimensions, far below the optical diffraction limit. While this is routinely used to manipulate light at the nanoscale,<sup>1</sup> in electro-optic devices<sup>2</sup> and enhanced spectroscopic techniques,<sup>3–6</sup> no characterization technique for imaging the underlying nanoscopic electromagnetic fields exists, which does not perturb the field<sup>4,7</sup> or employ complex electron beam imaging.<sup>8,9</sup> Here, we demonstrate the direct visualization of electromagnetic fields on patterned metallic substrates at nanometer resolution, exploiting a strong “autonomous” fluorescence-blinking behavior of single molecules within the confined fields allowing their localization. Use of DNA-constructs for precise positioning of fluorescence dyes on the surface induces this distance-dependent autonomous blinking thus completely obviating the need for exogenous agents or switching methods. Mapping such electromagnetic field distributions at nanometer resolution aids the rational design of nanometals for diverse photonic applications.

**KEYWORDS:** Super-resolution, single molecule localization, plasmons, nanostructures, surface-enhanced



Nanophotonics has evolved into a hugely interdisciplinary field at the interface of optics, materials, and nanoscience, with many applications in chemistry and biology.<sup>2</sup> Therefore, engineering well-defined nanostructured surfaces, which can sustain surface plasmon modes, is extremely important in technological applications such as enhancement of Raman scattering to permit the detection of single molecules<sup>10</sup> or to obtain reproducible characteristics for quantitative diagnostics.<sup>11</sup> Usually, the morphological characterization of such nanostructures is performed with scanning electron microscopy techniques.<sup>12</sup> However, only a few techniques allow the measurement of electromagnetic field distributions of plasmonic modes with nanometer resolution<sup>8,13</sup> without introducing field distortion. As a result, finite- and boundary-element simulations are widely used instead to predict field distribution on plasmonic surfaces, but this is associated with significant uncertainties and limitations. Simulation results are algorithm dependent and can only predict fields for idealized structures, which are free of imperfections, a situation never achieved in practice.<sup>14</sup>

Here we present a new technique, surface-enhanced localization microscopy (SELM), which does not suffer these

limitations and exploits the plasmonic enhancement of fluorescence combined with single molecule localization microscopy to resolve optical fields across nanostructured metal surfaces with 20 nm resolution.<sup>15,26</sup> To evaluate this resolution metric from the actual image data described in this Letter, the density estimation approach as explained in full detail in ref 26 was followed. We use a simple labeling technique to precisely position robust fluorescent dyes on gold surfaces via a DNA scaffold and show that this leads to “autonomous” blinking of the fluorophores. Unlike the conventional photochemical approaches to induce blinking of fluorophores for super-resolution microscopy externally through reagents or the photoactivation/excitation with a second laser wavelength,<sup>16–18</sup> we demonstrate here that the photodynamic response of standard fluorophores is considerably modified in the vicinity of nanostructured metal surfaces. The effect generates strong “autonomous” blinking of conventional fluorophores which is sufficient to localize them at high

**Received:** January 30, 2015

**Revised:** April 14, 2015

**Published:** April 27, 2015

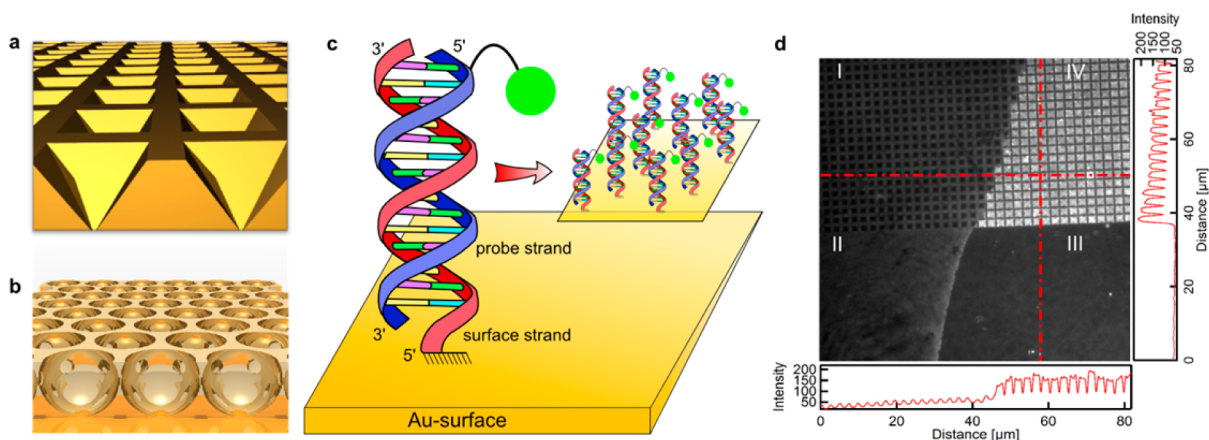


**Figure 1.** (a,b) Schematic representations of Klarite and nanovoid structured surfaces, respectively. (c) Sketch of the labeling technique involving two complementary DNA strands. The “surface strand” is attached to the surface by a thiol bond; the “probe strand” carries the dye molecule, here near its 5′ end. (d) Wide-field fluorescence image of a surface structure containing: (I) a platinum (Pt) plated pyramidal pit region, (II) a plain (nonstructured) Pt plated region, (III) a plain Au coated region, and (IV) an Au-coated Klarite surface. All regions were labeled with Cy5 positioned  $\sim 20$  nm above the surface (as in panel c). Only region IV supports surface plasmons, leading to the dramatically enhanced fluorescence signal seen. The red dash-dotted lines indicate sections along the surface for the two intensity profiles along the vertical and horizontal directions. The intensity profiles clearly show the enhancement in region IV compared to regions I and III.

resolution. Hence, super-resolution imaging by single molecule localization becomes possible without any requirement for chemical or optical control of fluorescent on- and off-states. Furthermore, by exploiting this autonomous switching, we are able to remove static interference efficiently, which otherwise impedes the correct localization of single emitters. We demonstrate that our powerful technique allows the mapping of nanoscopic EM field patterns in exemplar plasmonic structures, such as Klarite, featuring a pyramidal pit structure as shown in Figure 1a;<sup>19</sup> nanovoids, “dish-like” structures with variable diameter  $D$ <sup>20</sup> (Figure 1b); and random scratches on planar metal films. We find good agreement between experimental results of field distributions with the data obtained from finite element modeling. The simplicity of the SELM technique paves the way for its utilization in rational design of nanomaterials for diverse photonic applications including for all types of plasmon-enhanced spectroscopies.

In this work we utilize fluorescent dyes immobilized on metallic surfaces for demonstrating the SELM technique. Unlike Raman scatterers, fluorescent molecules can suffer from nonradiative electron transfer in the vicinity of metal surfaces, and this leads to quenching.<sup>24,25</sup> Thus, the maximum fluorescence emission is observed at a distance away from the surface due to the competition between nonradiative decay and field enhancement. In order to determine this distance empirically, we use dyes attached at different distal positions on double-stranded DNA (dsDNA) scaffolds (see Supporting Information). The fluorescent molecule is attached to a “probe strand” at a position near the 5′ end, which binds to a “surface strand” with a complementary sequence (Figure 1c). The surface strand is covalently attached to the metal. Using cyanine dyes, Cy5 and Hilyte 647, the optimal distance was found to be  $\sim 20$  nm, corresponding to attachment of the dye at the 53rd base-pair position above the surface. The dyes have excitation and emission maxima at 630 and 647 nm, respectively. A 642 nm laser was used for excitation, which is not only in resonance with the dyes but also with plasmons sustained on Klarite and nanovoids. The plasmon resonance in Klarite is very broad,  $>600$  nm, while nanovoids have stronger, tunable (size- and thickness-dependent) although less broad resonances. These

plasmonic properties of Klarite and nanovoid surfaces have been studied in detail earlier.<sup>19,21–23</sup> The fluorescence was detected at around 690 nm. Figure 1d shows a wide-field fluorescence image of Klarite, a commercially available substrate used for surface-enhanced Raman scattering (SERS). Strong fluorescence from Hilyte647 is visible in area IV, where the fluorescent molecules are attached with 20 nm linkers to the gold-coated pyramidal pit-structured surface. In contrast, regions I, II, and III, shown in the same image, exhibit only very dim (20–50 times less intense) fluorescence signals, originating from either nonstructured Pt (II) or Au (III) coated regions or Klarite coated with Pt (I). Only region IV supports plasmons, is brighter than the other regions, and thus clearly demonstrates their role on fluorescence signal enhancements.

For super-resolution imaging via single molecule localization one takes a large number of fluorescence images with sparsely distributed, blinking molecules and superimposes the reconstructed molecule positions. This then permits the structure of a labeled object to be resolved at nanometer precision<sup>17,26</sup> In our case, the dye density on the surface was controlled via the concentration of the probe strand. Incubating the surface for 10 min with a concentration of 100 nM dye-labeled probe resulted in less than  $\sim 15$  fluorescently active molecules per image frame (see Supporting Information, Figure S4). This was sufficient to permit the precise localization of individual fluorescent spots. We made sure that the surface was completely covered with “surface strands” and allowed the “probe strands” to attach randomly to avoid artifacts during imaging that might otherwise arise from fluorophore density variations (see materials and methods in Supporting Information).

For SELM on Klarite, image stacks of up to 10 000 frames, each with 20 ms integration time, were acquired. The Hilyte 647 dye was offset by 20 nm from the surface using the dsDNA scaffolding scheme (above). Intriguingly, we observed very strong fluorescence blinking of the dye (see Videos 1 and 2 of the Supporting Information). In our case this was observed in the absence of any photoactivation or addition of an external agent such as an aliphatic thiol, which is typically needed for stochastic optical reconstruction microscopy.<sup>27</sup> In addition, the photobleaching rate of the dye was drastically reduced (see

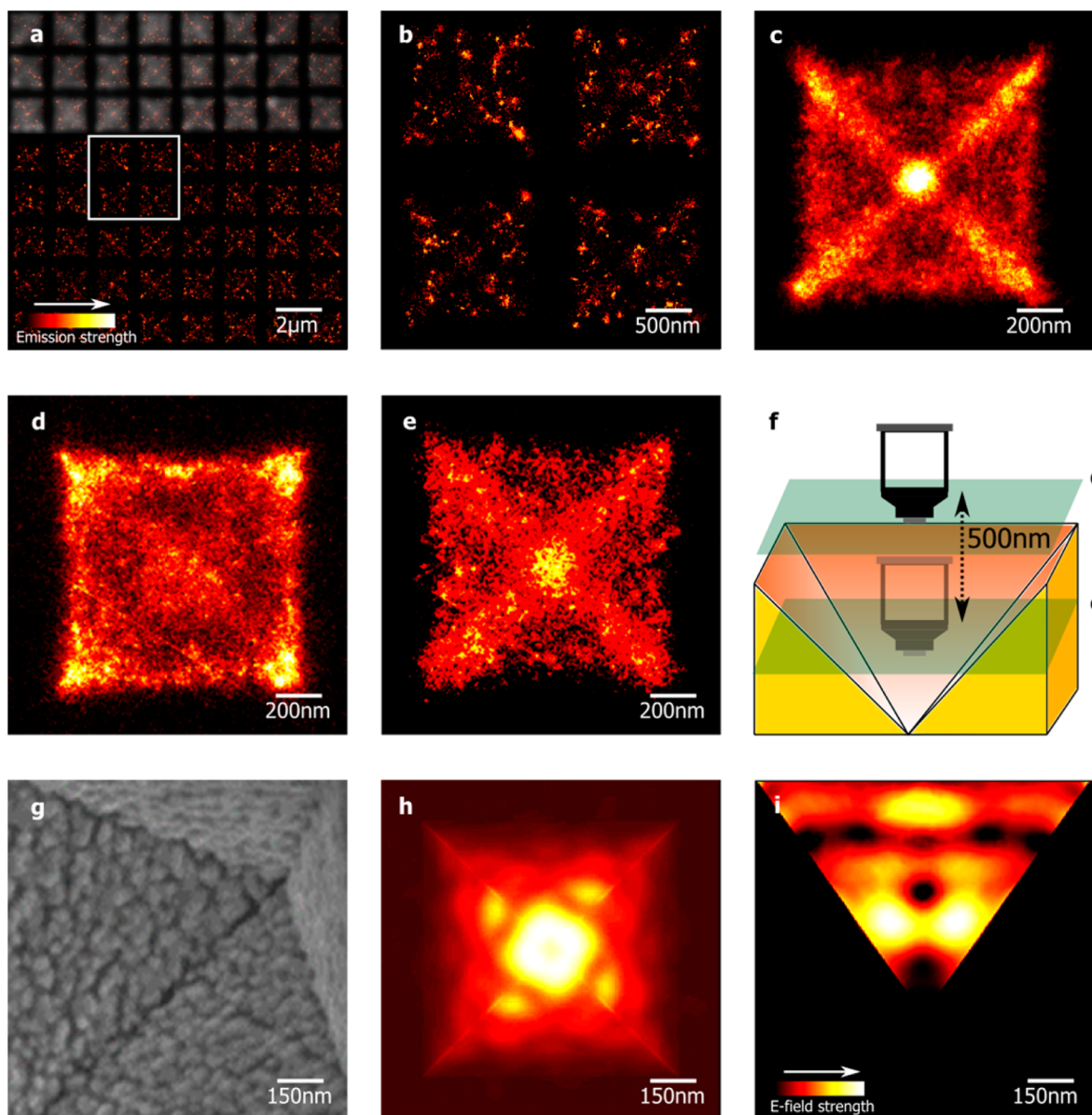


**Figure 2.** (a) Reconstructed SELM image of a Klarite substrate (red regions) and conventional, diffraction limited, wide field fluorescence image (overlaid as grayscale image in the top third of panel a). While the bright field image sees the coarse periodic structure of Klarite, SELM clearly resolves individual features inside the pits; the emission strength of individual localizations is color-coded. (b) Higher magnification view corresponding to the white inset shown in panel a. (c) Overlay image containing SELM reconstructions from 60 pits of panel a, revealing the strong enhancement along the edges and toward the bottom tip of the Klarite structure. The flat sides of the pit are less active. (d,e) SELM images at different focal heights inside a Klarite pit, which differ by 500 nm as indicated in panel f. Images show slightly more granular signals than in panel c as averages were taken over 25 pits only and the influence from the uncontrollable surface roughness is stronger. (g) Scanning electron microscopy picture at 20 degrees angle off the surface normal of a Klarite pit. The surface roughness is clearly visible from the image. (h,i) Finite element simulations of the electric fields inside a Klarite pit, see also the Supporting Information. (h) Vertically integrated view showing strong modes along the angled trough edges. (i) Vertical cut through a Klarite pit.

Supporting Information and videos). All these attributes are advantageous in the context of single molecule super-resolution imaging with SELM, and they are evidence of the dramatic modification of the dye properties in the proximity of the metal environment. In addition to dye fluorescence, a plasmon-enhanced gold photoluminescence was also observed. However, this static (nonblinking) background was removed effectively with a subtraction algorithm for improved localization (fitting) of the blinking observed from the dye (see the Supporting Information and Figure S4). It is also pointed out that the blinking behavior was not specific to Hilyte647 only

and was observed with Cy5 as well (data not shown); however, the dependence of molecular structure on the blinking behavior remains to be investigated.

Figure 2a shows the SELM images on Klarite, which is an array of square pyramidal microscale pits. Features within individual pits are clearly resolved, while the conventional bright field image only shows coarse structures. Features observed inside each pit resemble one another across the surface, an indication of the high reproducibility of the Klarite substrate geometry from pit to pit. In a highly magnified view (Figure 2b), however, finely distributed details of the generated

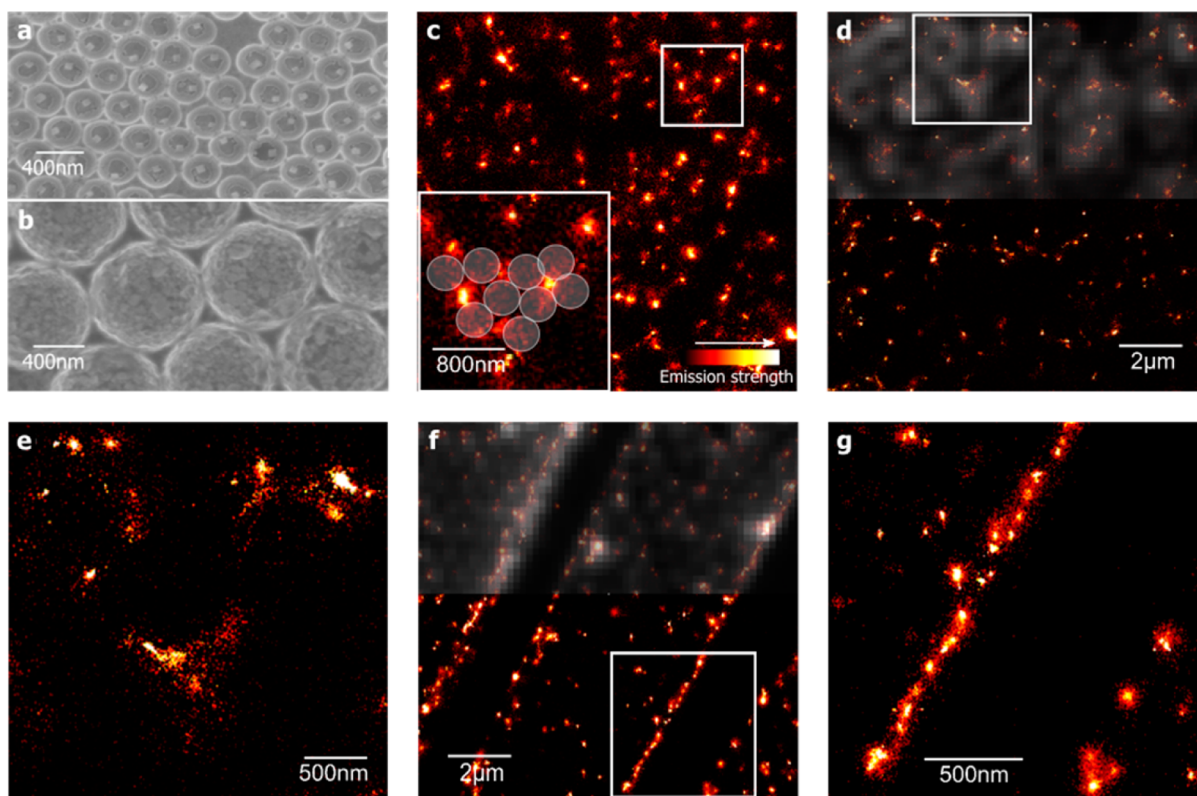


**Figure 3.** (a,b) SEM images of  $1\ \mu\text{m}$  and  $400\ \text{nm}$  nanovoids, respectively, the emission strength of individual localizations is color-coded. (c) Highly resolved SELM image of  $D = 400\ \text{nm}$  nanovoids showing a granular distribution of individual highly active spots. Unlike Klarite, enhanced fields on this sample do not show a clear pattern. The inset shows an expanded view and the possible location of the voids such that the hotspots imaged by SELM are at their intersections. (d) The SELM image of a labeled  $D = 1000\ \text{nm}$  void sample reveals a less dense distribution of such hotspots. Often, two or more “hotspots” are close together, as visible in the zoomed image in panel e. (f) Scratches on the surface (here  $D = 600\ \text{nm}$ ) are clearly visible as dark, nonactive areas. The edges of the scratch, however, show strong enhancements. (g) A zoomed in image of the scratch, inset in panel f, which reveals a high density of point-like spots along the edge in panel f.

surface enhanced fluorescence (SEF) are revealed. We attribute the “grainy” appearance of the monitored fields to the variable, uncontrollable surface roughness on the nanoscale, the latter borne out by SEM images as shown in Figure 2g.

An average over SELM images of many pits may therefore serve as an approximation to an idealized Klarite geometry, which features ultraflat surfaces. Strikingly, in the SELM image shown in Figure 2c, reconstructed by overlaying 60 different pits, intensities along the angled troughs increase much more than those along the walls of the pit and therefore appear highlighted in the images. Strong field modes are evident toward the bottom tip of the pit structure, as well along the angled edges. We note that these observations are highly reproducible for different Klarite samples. The other signals distributed in the pit remain at their original intensities but become more uniformly distributed within the frame, therefore confirming that they are stochastic and originate from the enhanced SEF signals due to the variable surface roughness. The SELM mapping thus highlights that although the geometry is key to generating field enhancements the surface roughness plays an important role in the overall field enhancements that occur in Klarite.<sup>28</sup> For comparison with the SELM image in Figure 2c, a conventional wide-field image was also reconstructed by overlaying the same 60 pits (see the Supporting Information, Figure S5). It is clear that the resolution of SELM is dramatically higher than that achievable with conventional wide field imaging. This demonstrates the ultrahigh sensitivity of SELM to visualize differences and

stochastic variations of field patterns at ultrahigh resolution in plasmonic structures. In Klarite we observe plasmons that appear as bright “hot” spots on SELM images, which are representative of field enhancements caused not only by the large-scale pit geometry but also by nanoscale surface defects. These features are normally not visible in simulations that cannot take surface roughness into account. They are also not resolved by traditional imaging methods, which probe averaged distributions at low resolutions.

To probe the plasmon fields in 3D by SELM we adjusted the confocal plane to correspond to different pit depth. SELM results for different imaging planes are shown in Figure 2d,e, respectively, clearly resolving stronger modes along the rims of the structures when the focal plane is positioned just above the surface plane. These angled trough edge modes also appear in simulations (Figures 2h,i). Strikingly, the simulations also predict a mode toward the bottom tip of the pit structure, corresponding to the strong mode seen experimentally in Figure 2c. There has been a lively debate in the recent literature regarding the position of this mode, predicting it to occur either in the middle of the pit or toward the bottom apex of the pit. Clearly we observe the latter here, which is in accordance with our own simulations as shown in Figure 2h.<sup>19,29,30</sup> The SELM technique proves directly the existence of a mode in close proximity to the bottom apex of the pyramidal pit, appearing as a highly confined region in Figure 2c,e. Less apparent in the simulations are the four angled edge modes that we observe experimentally along the trough diagonals. These modes are

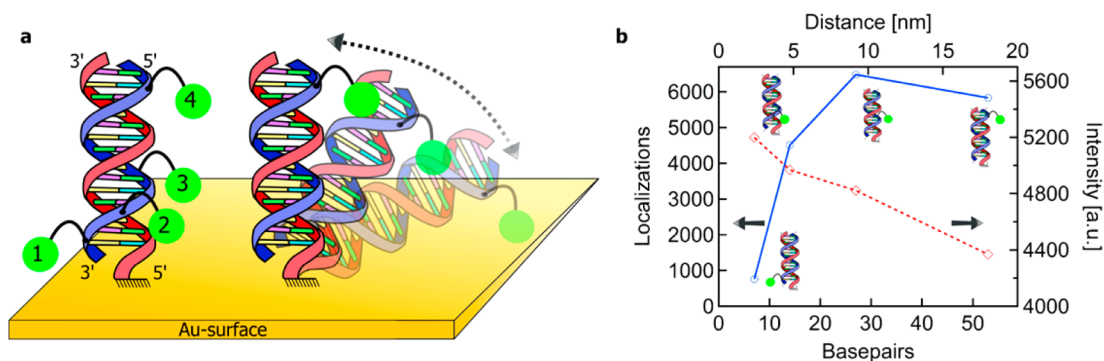


**Figure 4.** (a) Schematic showing DNA used as a nanoscopic ruler to vary the distance of a dye above the surface. Elastic bending of DNA causes blinking. (b) Localizations (number of blinking events) and their intensity per 4200 frames vs dye distance from the surface.

caused by imperfections in the pit structure that are likely to stem from the practical difficulty of depositing a metal coating uniformly across a sharp concave edge, resulting in momentum vector discontinuities for the generated plasmons, together with roughness. Both can give rise to a localized edge mode that is not captured by simulations. A further advantage of SELM is its wide-field imaging capability, which allows the identification of interactions between different plasmonic structures. In the case of Klarite, SELM confirms that there is no delocalization of plasmons between the neighboring pits.

In contrast to Klarite, super resolved SELM images of nanovoid structures as shown in Figure 3a exhibit remarkable differences, and only for very large diameters ( $D = 1000$  nm, Figure 3d,e) can the hotspots belonging to individual voids be distinguished. For  $D = 1000$  nm the interstitial ridges seem to support weak localized plasmons as apparent from the less intense and sparse SELM images. Individual hotspots are not well separated for void diameters of  $D = 400$  nm and  $D = 600$  nm (Figure 3c,f,g). Unlike Klarite, nanovoids are known to support delocalized plasmons propagating from one void to the next via the rim (edge) surface.<sup>21</sup> This “rim” mode has been shown to be significantly involved in generating SERS.<sup>21,31</sup> Hence, it is highly likely that localization occurs at the intersecting rims of three neighboring nanovoids in the hexagonal lattice. The intense bright regions or “hotspots” observed between neighboring voids pinpoint the high field strengths and highly confined plasmons, which give rise to strong SEF at the observed emission wavelength of the dyes. The plasmonic properties of nanovoids are easily tailored by varying the size of the sphere templates and their size.<sup>32</sup> The SEF enhancements observed are dependent on the plasmon resonances at both the excitation and emission wavelengths. For larger void diameters, the “hotspots” appear less dense (Figure 3c,f,g) as the plasmon resonances red-shift<sup>21</sup> and hence detune from the excitation and detection wavelengths used here. Interestingly, the scratch observed through the void surface shows a distinct topological boundary and generates highly localized spots of SEF, which are surprisingly strong and dense, but clearly resolved by SELM (Figure 3f,g). Such images of patterned substrates such as Klarite and nanovoids as well as nanostructures such as line scratch edges demonstrate that SELM is a generic method suitable for imaging plasmon fields in nanoscopic detail without requirements for complex photoactivation methods or external switching agents. One could argue that the orientational variations of fluorophore dipoles might cause misinterpretation of the data in terms of plasmonic field distributions. However, the DNA constructs are

minute compared to the dimensions of surface features, even those stemming from surface roughness. Thus, molecules are unhindered in their ability to change orientation, and thus, we do not expect the dipole orientations to be a function of molecule location across the substrate. While the orientation movements may differ, they will do so stochastically and should average out over the acquisition times (20 ms), orders of magnitude larger than reorientation time scales, and the many frames (up to 10 000) acquired in this work. Thus, the emission patterns given by SELM images represent averages over all permitted dipole orientations.

The simplicity of the SELM imaging method relies on the autonomous photon-blinking observed. Hence, this behavior was investigated further to establish whether quenching of the fluorophore (label) by the metal surface plays a role in the phenomenon. To test this, we varied the distance of the dye molecule, as shown schematically in Figure 4 by using different complementary strands. Thus, the labels were positioned at different heights above the surface by using the DNA as a scaffold (see also the Supporting Information). Image stacks of 4200 frames were processed for each type of fluorophore labeled strand and the number of localizations (blinking events) plotted versus linker length as well as the mean intensity of all individual localizations in a stack. The graph (Figure 4b) demonstrates that it is the number of on-off blinking events that decreases with decreasing fluorophore-metal distance rather than the intensity of each fluorescence event. The slight decrease of the number of localizations for a dye-surface distance greater than 10 nm can be attributed to decreasing intensities of individual blinking events with distance from the surface. Hence, photon bursts from single molecules with the fluorophore located further away from the surface have a higher likelihood of being not recorded by the algorithm employed by the rapidSTORM software used to analyze the photon statistics. In other words, as soon as a molecule is in the on-state, it is fluorescent and the fluorescence is as strong as permitted by the local electric field. The closer the fluorescent tag approaches the surface, however, the lower its probability to enter into an on-state. This leads us to suggest that the DNA strands (and/or the fluorescent labels attached to them) undergo orientational change (sway) on the surface due to Brownian motion, which has been observed previously.<sup>33,34</sup> The molecules’ tilt angles can change dynamically on the surface as in the elastic bending diffusion model developed previously.<sup>35</sup> Although we use low salt concentration (low ionic strength, high Debye length) and high pH (8.1) to increase the probability of upright orientations, such elastic bending could

still pivot around the hexa-ethylene glycol thiol linker used to anchor the dsDNA on the gold surface. The ultrahigh sensitivity of SELM on plasmonic surfaces enables us to visualize such motions. This dynamic bending, which moves the dye, couples two phenomena: it changes the distance to the surface, which varies (1) the strength of the optical field experienced and (2) the propensity for quenching. The strength of the field decreases further away from the surface, and quenching occurs only in close proximity to the surface as electrons can tunnel directly (nonradiative transfer) from the fluorophore to the metal. Thus, for dyes attached closest to the surface, positional changes are the smallest with respect to the surface; therefore, these will experience the greatest degree of quenching and thus have the lowest probability to be in a fluorescent on-state. Although quenching dominates the number of fluorescence events in this case, on occasion the fluorophore escapes the quenching regime bursts of very high intensity are observed because the plasmon field is strongest near the surface, leading to enhanced SEF. Moreover, because of the high field strengths associated with plasmons, dyes could be switched back into an on-state at any time without a chemical change of their environment. This would also explain the low rate of photobleaching observed (see Figure S7 in Supporting Information). While the autonomous blinking behavior removes the complexity of using external agents or photoactivatable fluorophores, the distance dependence of the blinking frequency also opens up other possibilities. Thus, SELM could be used in sensing and imaging of the 3D environment of molecules near metallic surfaces by coupling the distance-dependent frequency of blinking events to the hot-spot localization.

**Conclusion.** Surface enhanced localization microscopy (SELM) opens new possibilities to overcome conventional, diffraction-limited far-field scattering techniques to infer field distributions of nanoscopic plasmons. We have demonstrated the use of SELM for the direct visualization of plasmonic fields with nanometer resolution, which revealed plasmonic hotspots including those that arise from surface imperfections. SELM uses single molecule localization of surface-enhanced fluorescence but without the use of photoactivation or exogenous switching methods. The autonomous switching of fluorescence in SELM was found to depend on the distance from the metallic surface, which can potentially be utilized for super-resolution microscopy in 3D. This work paves the way for uncomplicated super-resolution microscopy of metallic nanostructures, useful in a wide range of fields including plasmonics, surface-enhanced spectroscopies, electrochemistry, and surface-science.

## ■ ASSOCIATED CONTENT

### Supporting Information

Materials and methods and supporting videos. The Supporting Information is available free of charge on the ACS Publications website at DOI: 10.1021/acs.nanolett.5b00405. The data supporting this paper can be accessed at <http://www.data.cam.ac.uk/>.

## ■ AUTHOR INFORMATION

### Corresponding Authors

\*E-mail: s.mahajan@soton.ac.uk.

\*E-mail: cfk23@cam.ac.uk.

## Author Contributions

C.S. performed all the experiments and analyzed all the results; M.E. implemented the setup and did all the simulations together with M.C. and G.S.; C.F.K. and S.M. conceptualized and supervised the project; C.F.K., S.M., and J.J.B. contributed to the materials, methods and techniques; C.S., S.M., and C.F.K. wrote the paper; all authors went through the paper and contributed to the results and discussion.

## Notes

The authors declare no competing financial interest.

## ■ ACKNOWLEDGMENTS

The authors would like to thank Sebastian van de Linde and Eric Rees for their contributions to super-resolution imaging. We acknowledge financial support from EPSRC grant EP/G060649/1, EP/H028757/1-2, EP/I012060/1, EP/L015889/1, MRC grant MR/K015850/1 and ERC grant LINASS 320503.

## ■ REFERENCES

- (1) Brongersma, M. L.; Shalae, V. M. *Science* **2010**, *328*, 440–441.
- (2) Ozbay, E. *Science* **2006**, *311*, 189–193.
- (3) Homola, J.; Yee, S. S.; Gauglitz, G. *Sens. Actuators, B* **1999**, *54*, 3–15.
- (4) Barnes, W. L.; Dereux, A.; Ebbesen, T. W. *Nature* **2003**, *424*, 824–830.
- (5) Aroca, R. F. *Phys. Chem. Chem. Phys.* **2013**, *15*, 5355–5363.
- (6) Fleischmann, M.; Hendra, P.; McQuillan, A. *Chem. Phys. Lett.* **1974**, *26*, 163–166.
- (7) Zayats, A. V.; Smolyaninov, I. I.; Maradudin, A. A. *Phys. Rep.* **2005**, *408*, 131–314.
- (8) Nelayah, J.; Kociak, M.; Stephan, O.; Garcia de Abajo, F. J.; Tence, M.; Henrard, L.; Taverna, D.; Pastoriza-Santos, I.; Liz-Marzan, L. M.; Colliex, C. *Nat. Phys.* **2007**, *3*, 348–353.
- (9) Nicoletti, O.; de La Peña, F.; Leary, R. K.; Holland, D. J.; Ducati, C.; Midgley, P. A. *Nature* **2013**, *502*, 80–84.
- (10) Kneipp, K.; Wang, Y.; Kneipp, H.; Perelman, L. T.; Itzkan, I.; Dasari, R. R.; Feld, M. S. *Phys. Rev. Lett.* **1997**, *78*, 1667.
- (11) Brown, R. J.; Milton, M. J. *J. Raman Spectrosc.* **2008**, *39*, 1313–1326.
- (12) Goldstein, J.; Newbury, D. E.; Joy, D. C.; Lyman, C. E.; Echlin, P.; Lifshin, E.; Sawyer, L.; Michael, J. R. *Scanning Electron Microscopy and X-ray Microanalysis*; Springer: New York, 2003.
- (13) Hofmann, C. E.; Vesseur, E. J. R.; Sweatlock, L. A.; Lezec, H. J.; Garcia de Abajo, F. J.; Polman, A.; Atwater, H. A. *Nano Lett.* **2007**, *7*, 3612–3617.
- (14) Barnes, W. J. *Opt. A: Pure Appl. Opt.* **2009**, *11*, 114002.
- (15) Rees, E. J.; Erdelyi, M.; Pinotsi, D.; Knight, A.; Metcalf, D.; Kaminski, C. F. *Opt. Nanosc.* **2012**, *1*, 1–10.
- (16) Rust, M. J.; Bates, M.; Zhuang, X. *Nat. Methods* **2006**, *3*, 793–796.
- (17) Heilemann, M.; van de Linde, S.; Schüttelz, M.; Kasper, R.; Seefeldt, B.; Mukherjee, A.; Tinnefeld, P.; Sauer, M. *Angew. Chem., Int. Ed.* **2008**, *47*, 6172–6176.
- (18) Lin, H.; Centeno, S. P.; Su, L.; Kenens, B.; Rocha, S.; Sliwa, M.; Hofkens, J.; Uji-i, H. *ChemPhysChem* **2012**, *13*, 973–981.
- (19) Perney, N.; de Abajo, F. G.; Baumberg, J.; Tang, A.; Netti, M.; Charlton, M.; Zoorob, M. *Phys. Rev. B* **2007**, *76*, 035426.
- (20) Baumberg, J. J.; Kelf, T. A.; Sugawara, Y.; Cintra, S.; Abdelsalam, M. E.; Bartlett, P. N.; Russell, A. E. *Nano Lett.* **2005**, *5*, 2262–2267.
- (21) Cole, R. M.; Baumberg, J. J.; Garcia de Abajo, F. J.; Mahajan, S.; Abdelsalam, M.; Bartlett, P. N. *Nano Lett.* **2007**, *7*, 2094–2100.
- (22) Mahajan, S.; Cole, R. M.; Soares, B. F.; Pelfrey, S. H.; Russell, A. E.; Baumberg, J. J.; Bartlett, P. N. *J. Phys. Chem. C* **2009**, *113*, 9284–9289.
- (23) Steuwe, C.; Kaminski, C. F.; Baumberg, J. J.; Mahajan, S. *Nano Lett.* **2011**, *11*, 5339–5343.

- (24) Lakowicz, J. R. *Anal. Biochem.* **2001**, *298*, 1–24.
- (25) Anger, P.; Bharadwaj, P.; Novotny, L. *Phys. Rev. Lett.* **2006**, *96*, 113002.
- (26) Rees, E. J.; Erdelyi, M.; Schierle, G. S. K.; Knight, A.; Kaminski, C. F. *J. Opt.* **2013**, *15*, 094012.
- (27) van de Linde, S.; Kasper, R.; Heilemann, M.; Sauer, M. *Appl. Phys. B: Lasers Opt.* **2008**, *93*, 725–731.
- (28) Gersten, J.; Nitzan, A. *J. Chem. Phys.* **2008**, *73*, 3023–3037.
- (29) Vernon, K.; Davis, T.; Scholes, F.; Gomez, D.; Lau, D. *J. Raman Spectrosc.* **2010**, *41*, 1106–1111.
- (30) Mechler, M.; Kukhlevsky, S. V.; Mechler, A.; McNaughton, D. *Phys. Chem. Chem. Phys.* **2011**, *13*, 20772–20778.
- (31) Mahajan, S.; Abdelsalam, M.; Suguwara, Y.; Cintra, S.; Russell, A.; Baumberg, J.; Bartlett, P. *Phys. Chem. Chem. Phys.* **2007**, *9*, 104–109.
- (32) Cintra, S.; Abdelsalam, M. E.; Bartlett, P. N.; Baumberg, J. J.; Kelf, T. A.; Sugawara, Y.; Russell, A. E. *Faraday Discuss.* **2006**, *132*, 191–199.
- (33) Chan, V.; Graves, D. J.; Fortina, P.; McKenzie, S. E. *Langmuir* **1997**, *13*, 320–329.
- (34) Rant, U.; Arinaga, K.; Fujita, S.; Yokoyama, N.; Abstreiter, G.; Tornow, M. *Nano Lett.* **2004**, *4*, 2441–2445.
- (35) Anne, A.; Demaille, C. *J. Am. Chem. Soc.* **2006**, *128*, 542–557.